EEG Instrumentation and Safety

7

Philip J. Allen

Abbreviations

AC   Alternating current
DC   Direct current
ECG   Electrocardiogram
EEG   Electroencephalography
emf   Electromotive force
EMG   Electromyography
EPI   Echo planar imaging
fMRI   Functional magnetic resonance imaging
MR   Magnetic resonance
MRI   Magnetic resonance imaging
RF   Radiofrequency
rms   Root mean square
SAR   Specific absorption rate

1
Introduction

The successful combination of electroencephalography (EEG) and fMRI demands careful consideration of three important issues: patient safety, EEG quality and image quality. In this chapter we first consider the implications these factors have on the design of EEG instrumentation, and then examine the precautions that must be taken in order that these recordings can be performed safely.

P. J. Allen
Department of Clinical Neurophysiology, The National Hospital for Neurology and Neurosurgery, Queen Square, London, WC1N 3BG, UK
e-mail: Philip.allen@uclh.nhs.uk

2
EEG Instrumentation

EEG instrumentation comprises electrodes, an acquisition system to amplify and digitise the EEG signals, and review facilities for the display and analysis of the recorded waveforms. The design of EEG instrumentation appropriate for use in the magnetic resonance (MR) scanner must take into account a number of factors that are not applicable to conventional EEG equipment: the presence of static and time-varying magnetic fields and their associated EEG artefacts; the need to limit radiofrequency (RF) emissions to preserve image quality; and finally the obvious requirement to avoid the introduction of ferrous materials into the scanner environment. These considerations dictate that EEG monitoring equipment used for diagnostic recordings in a clinical setting are not suitable for optimal EEG–fMRI monitoring. In this section, we examine the influence the above factors exert on the design of EEG instrumentation. We start at the beginning of the EEG signal chain with a consideration of the electrodes. EEG artefact post-processing correction methods are discussed in detail in the chapters "EEG Quality: Origin and Reduction of the EEG Cardiac-Related Artefact" and "EEG Quality: The Image Acquisition Artefact".

2.1
Electrodes

The term EEG electrode is used here to describe the combination of the electrode head and connecting lead. In addition to the EEG and image quality issues discussed in this section, EEG electrodes also raise safety issues when used in the MR scanner; these will be discussed in Sect. 3 of this chapter.

2.1.1
Electrode Lead Arrangement

The electromotive force (emf) induced in a conductive loop is proportional to the rate of change of magnetic flux cutting the loop and the loop area:

$$V_{induced} = A \times \frac{dB}{dt},\qquad(1)$$

where

$V_{induced}$ = emf induced in the loop,
A = loop area perpendicular to the field,
$\frac{dB}{dt}$ = rate of change of magnetic flux cutting the loop.

Hence, it is important to minimise the area of any loop formed by the electrode leads in order to reduce signal artefacts induced by the changing magnetic fields. A number of methods to achieve this have been reported (Goldman et al. 2000; Anami et al. 2003;

Hoffmann et al. 2000; Negishi et al. 2004; Vasios et al. 2006); in essence, these involve bunching electrode leads together at a single point on the head and then further minimising the loop area, typically by twisting the wires together as far as possible along their entire path from the subject's head to the amplifier inputs. This not only keeps the leads in close proximity to each other but also results in the cancellation of the induced emfs in adjacent twists. Nevertheless, EEG is recorded between separate points on the head, and hence some loop area is inevitable. Goldman et al. proposed minimising this by recording from a chain of linked bipolar pairs connected to individual differential amplifiers (Goldman et al. 2000). Although this can present a smaller loop than encountered in common reference recordings, it is more restrictive in terms of electrode placement, particularly when the number of channels is large. More common is the use of electrode caps, which combine the advantage of multichannel referential recordings with relatively low loop areas (Baumann and Noll 1999; Bonmassar et al. 1999; Srivastava et al. 2005; Laufs et al. 2003; Iannetti et al. 2002) (Fig. 1).

Although some groups have advocated shielding of the electrode leads (Hoffmann et al. 2000) and electrodes (Anami et al. 2003), presumably to reduce artefacts caused by electrostatic coupling to electric field sources in the scanner, a quantitative assessment of the benefit of this technique has not yet been reported. Minimisation of loop area is also important to ensure patient safety; this will be addressed in Sect. 3 of this chapter.
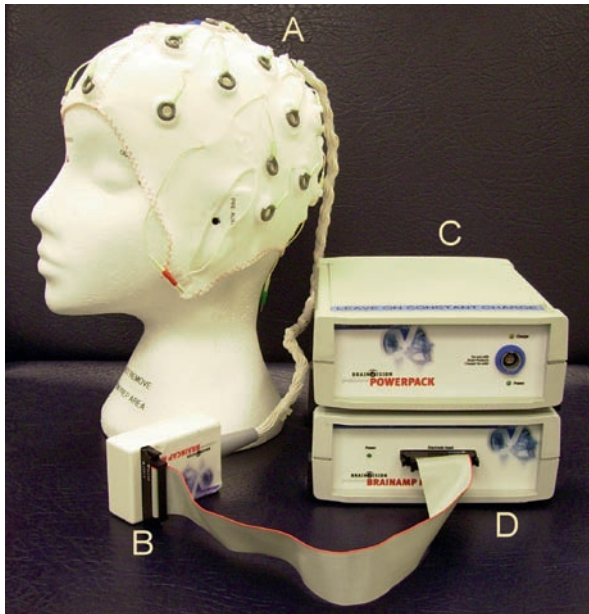
Fig. 1 Example of commercial EEG–fMRI instrumentation showing (**A**) electrode cap, (**B**) connector box containing current-limiting resistors, (**C**) battery power pack and (**D**) 32 channel EEG amplifier/digitiser. This instrumentation is sited adjacent to the scanner bore and transmits data to a receiver outside the Faraday shield via fibre optic links

2.1.2
Electrode Lead Movement

EEG artefacts are induced not only by changing magnetic fields cutting a static loop but also by variation in loop area in the static field. Such variation can result from the movement of the electrode leads caused by a ballistocardiogram (Debener et al. 2007; Allen et al. 1998), small head movements (Hill et al. 1995) and scanner vibration (Garreffa et al. 2004). A variety of methods have been used to minimise these artefacts, such as weighing down the electrode leads where they pass out of the scanner using sand bags (Benar et al. 2003), placing padding under the leads and amplifier (Hoffmann et al. 2000), placing a tight bandage over the patient's head to secure individual electrode leads (Benar et al. 2003), or the use of an electrode cap (Kruggel et al. 2000). There is general agreement that such fixation methods can reduce artefacts significantly.

Another important factor in reducing electrode lead movements (although not strictly part of the EEG instrumentation) is the reduction of patient head movement. Such immobilisation has been achieved using a vacuum cushion filled with polystyrene spheres (Benar et al. 2003; Anami et al. 2003). This method has been reported to be effective and well tolerated, the latter being an important factor in prolonged EEG–fMRI experiments, since any patient discomfort is likely to provoke gross movement, with its associated artefacts in both the EEG and magnetic resonance imaging (MRI) data.

In a comparison of three different methods for reducing lead and head movement (weighing down the leads, electrodes secured by a tight bandage, head fixed by vacuum cushion), Benar et al. found that the former was the most important and the vacuum cushion the least (Benar et al. 2003). It is interesting to note, however, that whereas artefact in the range 30–50 µV were observed for the subjects in this study, Kruggel et al. observed artefact of up to 500 µV using a broadly comparable arrangement (stretchable cap, twisted leads weighed down with rice bags, head restrained by cushions) (Kruggel et al. 2000). This tenfold difference (which cannot be attributed entirely to the different scanner fields in these studies, of 1.5 and 3 T respectively) suggests that these artefact minimisation techniques are very sensitive, and hence local experimentation may be necessary to find the optimal arrangement.

2.2
EEG Recording System

The EEG recorded in the MR scanner is contaminated by two different sources of interference that do not afflict clinical EEG recordings. The first is often referred to as pulse (or sometimes ballistocardiogram) artefact, and is caused by cardiac-related movement of the electrodes or blood flow in the static field. It is typically 10–100 µV in amplitude and overlaps the EEG frequency range (Allen et al. 1998). A variety of techniques have been developed to reduce these artefacts (Allen et al. 1998; Goldman et al. 2000; Bonmassar et al. 2002; Benar et al. 2003); these make no additional demands on the EEG instrumentation above those required for conventional clinical EEG.

The second source of interference is often referred to as imaging (or sometimes gradient) artefact, and represents the emfs induced in the electrode lead loops by the changing magnetic

fields applied during imaging. It has two distinct components, attributable to the gradient and RF fields respectively. The former range in frequency from the slice repetition interval (typically 10–20 Hz) up to the kHz range. The RF fields have a fundamental component at the Larmor frequency of the scanner, ranging from 63 MHz for 1.5 T up to 300 MHz for 7 T, but also lower-frequency components reflecting the rate at which the RF is pulsed (Hoffmann et al. 2000) and the pulse shape. In contrast to pulse artefact, imaging artefact is normally significantly larger in amplitude than the EEG, often obscuring the waveforms completely (Allen et al. 2000). In the early days of this technique, the EEG and fMRI were interleaved. In studies of epilepsy, this was typically achieved by triggering fMRI acquisition immediately after observing an epileptiform spike in the EEG (Warach et al. 1996; Seeck et al. 1998). It was accepted that the EEG recording during the image acquisition would be obscured. Subsequent developments in artefact subtraction methods have now made truly simultaneous EEG and fMRI recording routine. Although this makes greater demands on the EEG instrumentation, particularly with regard to filtering, sampling rate and dynamic range, it offers much greater freedom in experimental design and is now accepted as an essential requirement.

2.2.1
Filters

As RF artefacts occur at a frequency many orders of magnitude higher than those of EEG, they can be reduced to an acceptable level by low-pass filtering with a −3 dB cut-off point that is substantially higher than the EEG bandwidth. For example, Anami et al. demonstrated that a 3,000 Hz cut-off low-pass filter reduced the RF artefact to below 100 μV, substantially less than that of the gradient artefact (Anami et al. 2003) (Fig. 2). This filtering should, however, be implemented at the front end of the instrumentation to avoid possible demodulation of the RF into the EEG frequency range due to nonlinearities in subsequent active amplifier stages. Gradient artefacts, in contrast, overlap the EEG spectrum and hence cannot be removed by low-pass filtering alone. Nevertheless, analogue low-pass filtering prior to the main gain stage in the EEG amplifier is normally essential to prevent saturation by the high-amplitude gradient artefact. In order to maximise the attenuation of these artefacts, the cut-off frequency of this filter should be set as low as possible consistent with the recommended EEG bandwidth, typically 70 Hz (Deuschl and Eisen 1999). Attenuation of gradient artefact can be improved by using a higher-order (three or greater) analogue low-pass filter with a steeper roll-off. However, this comes at the expense of poorer phase-frequency linearity, which may result in distortion of EEG transients (Janssen et al. 1986) and hence should be avoided.

2.2.2
Sampling Rate

Given that low-pass filtering alone cannot remove all of the imaging artefact, a variety of post-processing artefact subtraction methods have been developed. The artefact removal method most commonly used to date is based on the subtraction of an artefact template
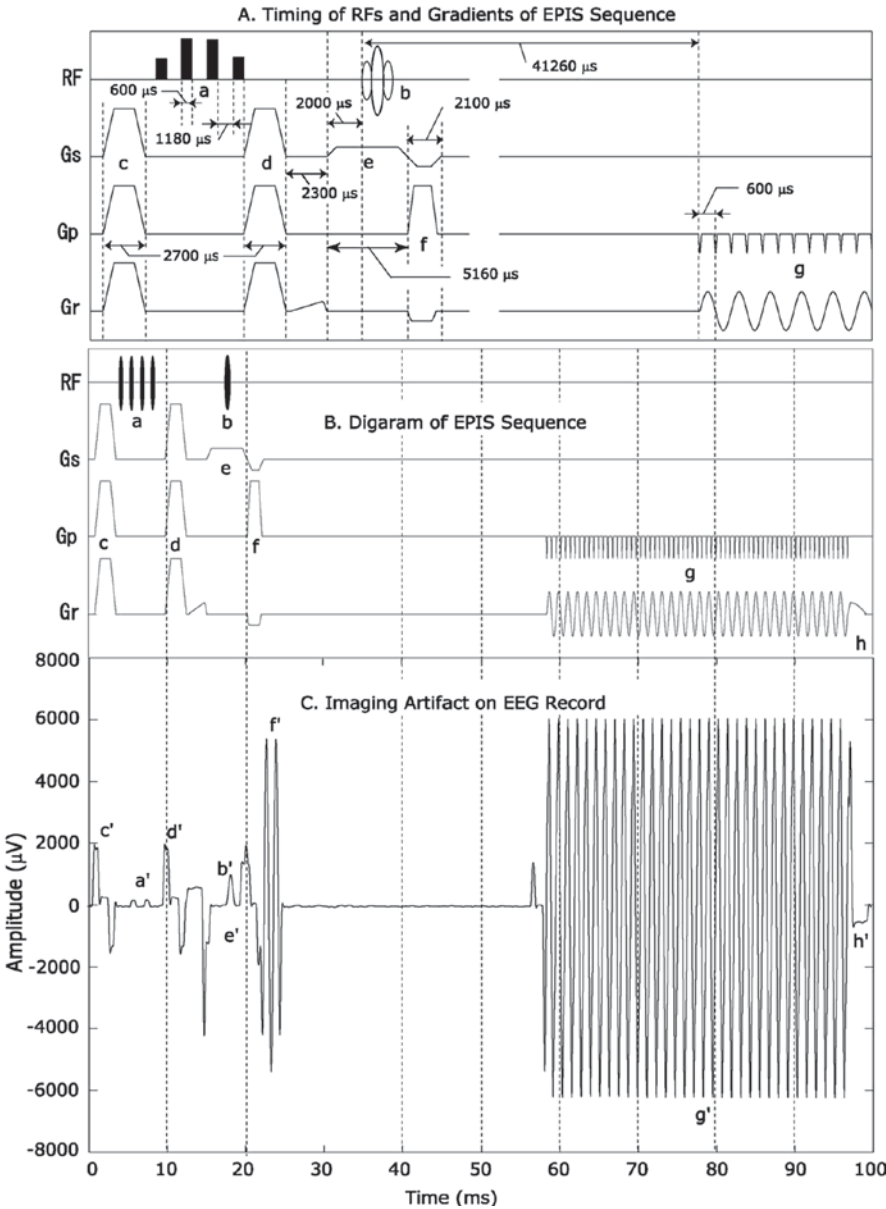
Fig. 2 **A** Timings of RF emission and gradient pulses in an fMRI sequence (EPIS, Siemens: ep2d_fid_60b2080_62_64.ekc). *RF*, radiofrequency wave; *Gs*, slice selection gradient; *Gp*, phase encoding gradient; *Gr*, readout gradient. *a*, Fat suppression pulses (1–3–3–1 pulses); *b*, slice selection RF; *c*, *d*, *h*, spoilers; *e*, slice selection gradient; *f*, dephasing and rephrasing gradient; *g*, readout gradient. **B** Schematic diagram of whole EPIS sequence. **C** Imaging artefact waveform for one slice scan on a dummy EEG record with a phantom using the EPIS sequence. The artefact corresponding to each gradient component described above in (**A**) can be identified, and is denoted by the same alphabet as that denoting the original gradient but with a prime. From Anami et al. (2003)

derived from averaging the artefact over a number of scan repetitions (Allen et al. 2000). Successful artefact subtraction by this method (and many of its subsequent enhancements; see for example Negishi et al. 2004; Benar et al. 2003) is dependent on accurate calculation of the artefact template. As the imaging artefact contains rapidly changing components, a fast sampling rate (typically 5 kHz) is required in order to capture these signals adequately (Allen et al. 2000). This is ten times higher than the rate used in conventional EEG equipment. Even at this high sampling rate, temporal jitter in the EEG sampling can lead to inaccuracies in the artefact template estimation that limit the effectiveness of this method (Cohen et al. 2001). Although technically feasible, increasing the sampling rate further results in very large datasets, especially for prolonged recordings using a large number of channels. Hence, an alternative approach has been proposed whereby the EEG sampling is synchronised to the MR scanner clock (Cohen et al. 2001). Mandelkow et al. demonstrated that this method can reduce the residual artefact, particularly the higher-frequency EEG components, and achieves good artefact reduction even when using a conventional EEG sampling rate of 500 Hz (Mandelkow et al. 2006). It is worth noting, however, that the EEG in this study was originally sampled at 5 kHz then down-sampled to 500 Hz after the application of a seventh-order digital filter, an important step for preventing aliasing. As the authors comment, the application of such a high-order filter implemented in hardware prior to digitising at 500 Hz would inevitably distort the EEG due its nonlinear phase response. Nevertheless, the method holds great promise for improving artefact suppression, particularly when there is a requirement to analyse higher-frequency EEG components such as the gamma bands. It therefore follows that the facility to synchronise the EEG sampling rate precisely to an external clock is a useful addition to the EEG instrumentation specification. This synchronisation also requires hardware to reduce the scanner clock to the EEG sampling rate (10 MHz to 5 kHz in the report by Mandelkow), but this can be achieved independently of the EEG instrumentation, for example by phase-locked loop circuitry (Mandelkow et al. 2006) or a clock divider.

2.2.3
Signal Range

The amplitude of gradient imaging artefact in the EEG is proportional to the loop area and the rate of change of magnetic flux cutting the loop, as described in Eq. 1. Allen et al. calculated that for a relatively high slew rate of 125 T m^{-1} s^{-1} and a worst case EEG lead loop area of 100 cm^2 located 0.2 m from the scanner isocentre, the induced artefact due to gradient fields is ±250 mV (Allen et al. 2000), more than two orders of magnitude greater than the recommended range (±1 mV) for conventional EEG equipment (Nuwer et al. 1999). In practice, careful alignment of electrode leads can help reduce the artefact amplitude substantially. Anami et al. recorded imaging artefact from electrodes on a phantom in a 1.5 T scanner using a typical blipped echo planar imaging (EPI) sequence (see the chapter "EEG Quality: Origin and Reduction of the EEG Cardiac-Related Artefact"), wide bandwidth [direct current (DC) to 3,000 Hz] and 20 kHz sampling (Anami et al. 2003). This revealed a substantially lower maximum gradient artefact of 40 mV (Fig. 2). However, the use of faster slew rates or the acquisition of different physiological parameters such as electrocardiogram (ECG) and electromyography (EMG), which may necessarily involve larger loop areas, would result in proportionally larger artefact. It is therefore still important that the EEG instrumentation has

sufficient range throughout the entire signal path to record these signals without saturating—if the artefact saturates then the underlying physiological signal will be lost. It is important to note that saturation is not always obvious by inspection of the recorded EEG signal, due to the effect on the waveform of subsequent circuit stages such as alternating current (AC) coupling and additional high- and low-pass filters. The following factors need consideration when assessing whether EEG instrumentation has sufficient range: the amplitude and spectral distribution of the imaging artefact, the frequency response and location in the overall system of the analogue low-pass filters, and the signal range at each stage of the EEG instrumentation. For example, Allen et al. described an EEG amplifier with an overall dynamic range in the passband of 33.3 mV, which, through the judicious use of gain and filter stages, could handle artefact of ±250 mV pk–pk at source without saturating (Allen et al. 2000).

2.2.4
Signal Resolution

In addition to providing sufficient signal range, the EEG instrumentation must also have adequate resolution. The minimum recommended resolution for conventional EEG equipment is 0.5 µV (Nuwer et al. 1999). Given the need for a large signal range of the order 20–30 mV as described above, this resolution would require 16 bits, which in practice requires a digitiser with more than 16 bits. However, given that the residual artefact from current pulse- and imaging-artefact subtraction methods is at least 5 µV (Allen et al. 2000), and that this error occurs independent of digitisation errors, 16-bit digitisation yielding 14–15 effective bits and hence a resolution of 1–2 µV is adequate. As artefact subtraction methods improve, greater bit depth may be justified, especially when recording lower-amplitude EEG activity such as event-related potentials (ERPs). The dynamic range can, however, be increased for these by averaging, albeit at the expense of longer recording time.

2.3
RF Emissions

The MRI scanner contains an extremely sensitive RF detector. Any RF emissions from the EEG instrumentation may lead to artefacts in the MR images if they fall in the frequency range detected by the scanner. Potential sources of these emissions are active circuitry in EEG instrumentation located in the scanner room or the ingress of RF signals via conductors that breach the scanner's Faraday shield. For the former, careful design is required to minimise RF emissions, as even relatively low-frequency digital circuitry can generate signals in the RF range due to the presence of harmonics. These may pass into the head coil by conduction along the electrode leads or by radiation through space. A number of techniques can be used to minimise this interference: RF signals should be minimised at source by using low-power digital components, thereby minimising switching currents; all active circuitry should be enclosed in a conductive enclosure (Allen et al. 2000; Gualniera et al. 2004; Garreffa et al. 2004); and all conductive signal paths (for example connections to EEG electrodes and external battery packs) breaching this enclosure should do so via in-line RF filters (Fig. 3). Where active EEG instrumentation is located in the scanner room,
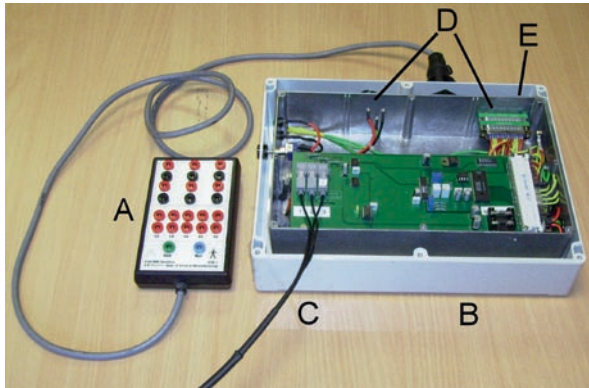
Fig. 3 Example of early in-house MRI-compatible EEG instrumentation developed in 2000 by our group. *A*, Nonferrous electrode connector box suitable for mounting in the bore of the magnet. *B*, EEG amplifier and digitiser; *C*, fibre optic cables transmitting digitised EEG data to a receiver unit outside the scanner room; *D*, in-line RF filters fitted to all signal lines breaching the shielded enclosure; *E*, shielded enclosure limiting RF emissions

EEG data is normally transmitted to a receiver in the console room via fibre optic cables, thereby eliminating the ingress of RF from outside the scanner (Figs. 1 and 2). This approach has been implemented in a number of commercial products.

Alternatively, the EEG instrumentation can be sited in the console room, with connection to the subject made via long electrode leads which pass through the Faraday shield (Huang-Hellinger et al. 1995; Anami et al. 2003). If the impedance of these leads is low, RF filtering must be applied at the point where the electrode leads breach the Faraday shield (Huang-Hellinger et al. 1995). Careful consideration must also be given to the safety implications of using such long cable runs with direct electrical connection to the patient, especially with regard to the accidental application of external voltage sources to these cables.

As stated previously, RF emissions will only cause image artefacts if they fall in the frequency range detected by the scanner receive coil and within the receiver bandwidth used for the imaging experiment, which occupies a narrow range either side of the Larmor frequency. Hence, it is perfectly possible that EEG instrumentation that does not generate image artefact when used with one scanner may cause interference in another. Hence, an empirical test of image artefact should be undertaken prior to introducing new EEG instrumentation.

2.4
Miscellaneous Factors

In addition to the essential characteristics described above for high-quality EEG recording in the MR scanner, EEG equipment should broadly meet the requirements for conventional EEG. The key parameters are as follows: maximum noise at input of 1.5 μV pk–pk; bandwidth 0.16–70 Hz, input impedance $\geq$100 MΩ; common mode rejection $\geq$110 dB (Nuwer et al. 1999). A DC input range of ±300 mV is sufficient to handle the likely range of electrode potentials (Kamp and Lopes Da Silva 1998). Built-in electrode impedance

checking and a 50/60 Hz notch filter are desirable. Finally, the EEG review facilities should not be overlooked. Although the conventional requirements such as remontaging flexible sensitivity and time base must obviously be provided, one specific additional requirement for EEG–fMRI instrumentation is the facility to correlate (e.g. mark and export) specific EEG events the corresponding fMRI data simply and accurately.

2.5
Summary

The 15 years that have passed since the first reported recording of EEG during fMRI (Ives et al. 1993) have seen a burgeoning of interest in this technique. This has prompted the commercial development of EEG instrumentation designed specifically to meet many of the technical requirements described above, further extending the availability of the technique. Although further improvements in artefact minimisation would be desirable to record lower-amplitude activity such as ERPs or fast gamma activity, an EEG quality appropriate for studies of epilepsy and basic EEG rhythms can readily be achieved. However, it remains essential to pay careful attention to the entire recording setup comprising the subject, electrodes and EEG recording system in order to achieve optimal EEG signal quality. This will become even more important as higher-field scanners and studies of more subtle EEG activity become increasingly common.

3
Safety

Recording EEG in the MR scanner raises important safety issues. First, there is the hazard associated with the introduction of ferromagnetic materials into the scanner. Secondly, currents induced in the electrodes and attached wires by the changing fields applied during imaging can present a hazard due to the following mechanisms: eddy current heating of the electrode heads; currents induced in loops formed between the electrode leads; and currents induced along electrode leads. The safety implications of induced currents are determined by the field frequency, with different biological mechanisms for damage for the gradient- and RF-related fields. We begin by considering the relevant safety limits before moving on to a more detailed examination of each specific hazard.

3.1
Safety Limits

In the absence of a safety standard specifically addressing combined EEG–fMRI, the onus has been on users of this technique to demonstrate compliance with the standards applicable individually to MR and EEG equipment. Hence, the following safety limits derived from these standards apply: (1) maximum permissible cerebral temperature of 38°C,

implying a maximum temperature increase due to scanner induced heating of 1°C (IEC 2002a); (2) maximum permissible temperature of an applied part in skin contact (such as an electrode) of 43°C (IEC 2005); and (3) maximum permissible tissue contact currents ranging from 0.5 mA rms (≈1 kHz) to 10 mA rms > 100 kHz (IEC 2005).

In addition, EEG instrumentation must meet the safety requirements for general medical electrical equipment (IEC 2005) and the particular standard for EEG equipment (IEC 2002b).

3.2
Static Field

The principal safety issue associated with the static field is the force it exerts on ferromagnetic material. Fortunately, this is not a significant limitation since there are a range of nonferromagnetic materials that meet the requirements for high-quality EEG. These include combinations of silver, silver chloride, gold, carbon and conductive plastic for scalp recordings, and iridium/platinum for intracerebral recordings. However, care should be taken to exclude the presence of ferromagnetic material in ancillary items, such as securing springs in electrode caps or amplifier connectors. Stainless steel sphenoidal electrodes are clearly unacceptable.

Any new EEG instrumentation introduced into the scanner must also be tested for displacement force and torque (Baumann and Noll 1999; Woods 2007). In addition, it should be noted that any electronic components dependent on ferromagnetic behaviour (such as some switching DC-DC converters, ferrites) may not function when placed in close proximity to the static field.

One further potential hazard is the current induced in an electrode lead loop moved through the nonuniform region of the static field, for example when the patient is introduced into the scanner. This current will flow between electrodes and hence through the patient. Lemieux et al. investigated this at 1.5 T and identified that the effect was very small and hence no additional safety measures were required (Lemieux et al. 1997), although this may require reassessment with the development of higher-field shielded magnets.

3.3
Gradient Fields

The emf induced in an electrode lead loop by the gradient fields is proportional to the rate of change of magnetic flux cutting the loop and the loop area, as defined in Eq. 1. As the frequency of these fields typically does not extend much higher than 1 kHz, the dominant physiological effect is neuromuscular stimulation. Lemieux et al. calculated that for a relatively high slew rate of 120 T m^{-1} s^{-1} and a worst case loop area of 400 cm^2, loop resistance must be at least 3.3 kΩ in order to meet the safe limit of 0.5 mA rms under a single fault condition, namely the electrode leads accidentally shorting together (Lemieux et al. 1997). As a much higher value of current limiting resistor is normally required to limit heating

due to RF-induced currents, this does not present an additional constraint. Indeed, the inevitable tissue contact impedance presented at each electrode (of the order of 1 kΩ), combined with careful electrode lead arrangement to reduce the loop area below the pessimistic 400 cm^2, means that the current limit requirements can feasibly be met even if a current limiting resistor is omitted. However, this would need further consideration if substantially higher slew rates were used or loop area was increased, for example by recording from very widely spaced possibly noncephalic electrodes.

3.4
Eddy Currents

The RF fields applied during scanning induce eddy currents in the electrodes (Lemieux et al. 1997). These currents are much greater than those induced in human tissue, due to the relatively higher electrical conductivity of the electrode material, and may result in Joule heating of the electrode (Roth et al. 1992). Lemieux et al. investigated eddy current heating of a silver/silver chloride electrode in a 1.5 T scanner [averaged specific absorption rate (SAR) 0.06 W/kg] and found a maximum temperature increase of <1°C, comfortably within the permitted limit (Lemieux et al. 1997). Similar results have been found at higher field strengths: Mirsattari et al. found no temperature rise in a gold-plated pure silver electrode in a 1.5 T scanner (averaged SAR up to 1.6 W/Kg) (Mirsattari et al. 2004); Stevens et al. found no significant heat increase in the same electrode or in a silver/silver chloride in carbon embedded plastic electrode at 4 T with a high-power pulse sequence (8 W average per TR) (Stevens et al. 2007).

There is, however, evidence that eddy current heating may prove more significant at 7 T: Vasios et al. recorded a 2.2°C rise in a full-ring electrode following 22 min of high-power turbo spin echo (TSE) with a maximum local SAR of 11 W/Kg (Vasios et al. 2006), a power level just above the maximum SAR limit (IEC 2002a). Although this heating may not be due entirely to eddy currents (the temperature increase was recorded from a 32 electrode configuration and hence would include heating effects from currents induced in the associated conducting loops and elongated conductors), these clearly made a significant contribution since the temperature rise for the same configuration was reduced to 0.8°C when the full-ring electrodes were replaced with half rings designed specifically to reduce eddy currents.

In summary, these experimental investigations indicate that at field strengths of 4 T or less, electrode heating due to eddy currents does not appear to pose a risk to patients. Above 4 T, more specialised electrode design and/or SAR limits may be required. See the chapter "Specific Issues Related to EEG–fMRI at B_0 > 3 T" for further discussion.

3.5
RF Fields

The dominant physiological effect of induced high-frequency currents (>100 kHz) is tissue heating. The interaction between the scanner's RF (B_1) field and electrode leads can result in heating via two related mechanisms. Firstly, the magnetic component of the B_1 field will

induce an emf in any conductive loop formed by the electrode leads. This emf is proportional to the loop area cut by the field and the rate of change of the field (1). If tissue forms part of the loop, the induced emf will drive a current through this, causing heating. It is worth noting that in contrast to gradient field induced currents, the capacitance between bundled electrode leads presents relatively low-impedance conductive loops at RF frequencies, even if the leads are not accidentally shorted together, i.e. the non-fault condition (Lemieux et al. 1997). Secondly, the electric component of the B_1 field can induce a current along the extended conductor formed by an electrode lead (the antenna effect). The magnitude of this current is influenced by a wide range of factors, including the proximity of the wires to the source of electric field in the MR transmitter coil (Hofman et al. 1996) and the resonant length of the electrode leads in relation to the RF wavelength, with a theoretical maximum induced current for multiples of half wavelength (Pictet et al. 2000). As a broad guide, the resonant length of a straight wire in air is 2.35 m at 1.5 T and 1.17 m at 3 T (Dempsey et al. 2001), but this varies significantly according to the wire diameter, shape, insulation thickness and permittivity, and tissue conductivity and permittivity (Yeung et al. 2002). Although it is known that the maximum temperature increase associated with these currents occurs in tissue adjacent to the tip of a conductor, where the electric field is maximum (Yeung et al. 2002), accurate prediction of the associated temperature rise for a given scenario remains problematical. Both mechanisms for interaction of the electrodes and leads with the scanner RF fields are exacerbated by resonant conditions where the induction of much larger currents occurs (Dempsey et al. 2001); it is thus necessary to avoid these conditions.

In the first systematic study of safety due to RF heating of EEG electrodes in the MR scanner, Lemieux et al. investigated induced currents due to the electric and magnetic fields separately and concluded that the latter dominated and that a current-limiting resistor (12 kΩ) was required in the scalp electrode leads in order to limit contact currents to acceptable levels for a worst case electrode lead loop (400 cm^2) and high SAR for a 1.5 T scanner (Lemieux et al. 1997). This additional resistance is small relative to the typical input impedance of an EEG amplifier (at least 10 MΩ) and hence does not degrade EEG signal quality significantly. This study was undertaken using a head RF transmit coil—the safety of EEG–fMRI for body RF coils has not yet received a thorough investigation. The authors stressed the importance of performing a local risk assessment of the specific electrode and scanner setup using the methodology presented. Data supplied by the manufacturer on the relationship between B_1 and SAR for the quadrature transmit and receive head coil used in the GE Signa Excite 3 T scanner demonstrates that the RMS value of B_1 for a given SAR value (and body weight) is less than 50% of the value at 1.5 T, and therefore so will be the current induced in the EEG system-patient circuit, suggesting that the proposed safety measure is also adequate for this instrument, even taking into account the effect of the higher RF frequency.[1]

Our group has performed over 300 EEG–fMRI recordings at both 1.5 and 3 T using electrodes with current limiting resistors without incident. Current limiting resistors are included in a number of commercial electrodes and electrode caps designed for

---

[1]This corresponds to the fact that more heating is induced per unit B_1 at 3 T than at 1.5 T. The lower expected induced currents reflect the fact that the regulatory SAR limits are independent of field strength.

EEG–fMRI. Such studies have been performed at multiple centres worldwide over the last ten years; as far as the author is aware there have been no reports of adverse incidents resulting from these recordings. It has been proposed, on the basis of in vivo temperature measurements in a small number of subjects for a particular experimental setup, that additional resistors are not in fact necessary (Lazeyras et al. 2001). However, their use does provide reassurance that even under worst-case conditions (including a single fault), the subject will not be harmed, with only a minimal associated increase in EEG noise.

An alternative approach to establishing the safety of RF/EEG electrode interactions is the measurement of temperature changes during the scanning of electrodes attached to a head phantom. This method has been used extensively in the safety assessment of implants in the MR scanner (Carmichael et al. 2007a; Baker et al. 2004; Yeung et al. 2002; Gray et al. 2005) and more recently for EEG electrodes (Vasios et al 2006; Angelone 2006). The reliability of the temperature changes recorded using this approach is of course strongly influenced by the accuracy of the physical model. In particular, the head phantom must have realistic geometric, thermal and electrical properties (Angelone et al. 2006; Rezai et al. 2002; Park et al. 2003). Although the absence of thermoregulation from the head models used to date is clearly an inaccuracy, this merely leads to a conservative estimate of the temperature increases expected in human studies (Akca et al. 2007). The electrode lead length is also important: Yeung et al. observed substantial differences in heating at the tip of a length of wire in response to small changes in its length (of the order of a few centimetres) (Yeung et al. 2002). Similarly, the proximity of conducting leads to the transmit coil (where the electric component of the RF field is maximal) can affect heating significantly (Dempsey et al. 2001; Georgi et al. 2004). It is also important to use electrode gel in order to accurately replicate the electrical contact between the phantom and electrode (Vasios et al. 2006). The precise location of a temperature probe in the electrode gel can also introduce significant measurement variability (Angelone et al. 2006). In summary, careful experimental technique combined with a knowledge of the wide range of factors that influence MR-induced heating is an essential prerequisite for a reliable safety assessment based on this methodology (Shellock 2007). Finally, it is important to note once again that measurements performed on one scanner are not transferable to other scanners, and hence a local assessment combined with strict adherence to an experimental protocol is essential (Kainz 2007; Carmichael et al. 2007a).

One limitation of this empirical approach is the restricted spatial sampling that can be achieved with current MR compatible thermometry (typically four sites). This requires assumptions to be made regarding the location of the greatest temperature rise, which may be difficult to predict with certainty for a particular arrangement of electrode and leads in the scanner. One potential solution is to calculate temperature changes from a computational simulation of the electric field distribution resulting from the application of RF fields to a realistic head/electrode model. This approach allows the direct visualisation of the local SAR (and hence by application of the heat equation, the associated temperature changes; Collins et al. 2004) throughout the entire head volume, rather than just at selected sites.

Angelone et al. have used this method to investigate RF heating of EEG electrodes at 7 T (Angelone et al. 2006). Electric field and SAR values were calculated using the finite difference time domain method applied to numerical models of the electrodes, leads, RF coil and anatomically accurate homogeneous head model. The simulated temperature changes were validated by comparison with those measured for an equivalent electrode/phantom head

arrangement in the scanner, the two methods showing broad agreement in spatiotemporal distribution of temperature change. A maximum temperature rise inside the head of 3.4°C (i.e. above the 1°C safe limit) was identified for a high-power TSE sequence, indicating the need to limit SAR below the normal maximum permissible level (IEC 2002a). Interestingly, the authors found minimal difference between the simulated SAR distributions for electrodes with and without a modelled current limiting resistor. It is possible that at such high frequencies (300 MHz for 7 T), parasitic capacitance in the resistor reduces its impedance, thereby limiting its current limiting capability. This suggests that discrete current reducing resistors may not provide effective protection against SAR increases inside the head at 7 T, although their effect on contact currents, which might be expected to be maximal immediately adjacent to the electrodes (i.e. on the surface of the phantom), was less clear. Lower-temperature increases were recorded when using carbon leads, suggesting that distributed resistance in the electrode leads may be advantageous. See the chapter "Specific Issues Related to EEG–fMRI at $B_0 > 3$ T" for further discussion of the specific issues related to high-field EEG–fMRI.

Carbon leads may also reduce magnetic susceptibility artefacts in the images (Van Genderingen et al. 1989; Van Audekerke et al. 2000). Although promising, the use of computational simulation to assess the safety of RF/EEG electrode interactions is relatively new: further validation is required before this technique can be used on its own to establish patient safety. Combining this computational method with temperature measurement in a comparable physical model may prove advantageous, with the former being used to identify the site of maximum heating and the latter to verify the temperature changes at the equivalent position in the physical model.

Finally, although many studies have recommended the use of SAR limits to ensure the safety of EEG–fMRI experiments (Angelone et al. 2004; Lemieux et al. 1997), such limits are both scanner- and RF coil-specific. Indeed, Baker et al. have demonstrated that the relationship between scanner-reported SAR and the associated heating of an implanted electrode can be highly variable, even between scanners of identical field strength from the same manufacturer (Baker et al. 2004). It is likely that this is also the case for scalp EEG electrodes, and hence it is important to recognise that a universal SAR limit calculated for a specific electrode set, although attractive in its simplicity, may not be reliable.

3.6
Implanted Electrodes

The above discussion of safety issues has only addressed scalp electrodes. Imaging for postsurgical localisation of intracranial electrodes is currently performed in a number of centres. Retrospective examination of patients with implanted electrodes who underwent MR imaging indicate that the risks are generally low (Davies et al. 1999; Brooks et al. 1992). In addition, a small number of studies have investigated the safety of imaging implanted electrodes and found no evidence of displacement force and RF heating beyond safe limits (Boucousis et al. 2005; Kanal et al. 1999). However, these studies only investigated single electrodes, whereas in practice these recordings involve multiple electrodes, thereby introducing interelectrode lead loops. More recently, Carmichael et al. measured RF heating for a combination of subdural strips and depth electrodes at 1.5 and 3 T (Carmichael et al. 2007b). This
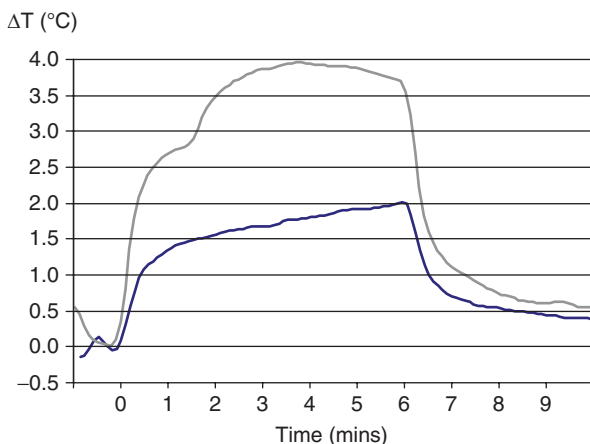
Fig. 4 Temperature increase with time for a subdural grid electrode contact, high SAR (2.4–2.5 W/kg). The *grey line* shows the temperature rise when all the electrode tails were in electrical contact, the *blue line* when they were all separated

showed that, for high SAR ($\approx$2.5 W/kg), the worst case temperature increase only exceeded the 1°C limit at 1.5 T when the electrode tails were shorted together (contrary to the manufacturer's recommendations); at 3 T the limit was exceeded even when the tails were isolated (Fig. 4). Clearly, a local investigation of temperature increases for a given specific electrode arrangement, scanner and pulse sequence is essential in order to identify the safe SAR limit.

This study (Carmichael et al. 2007b) only investigated the safety of electrode/RF interactions for MR-based electrode *localisation*. Recording from intracranial electrodes may be important in the application of EEG–fMRI to epilepsy. However, recording EEG from these electrodes during MR requires additional cabling to link the electrodes (which typically have tails of only 30 cm in length) to the EEG amplifier. Such conductors are likely to alter the resonant length of the overall EEG electrode assembly, potentially modifying the associated temperature changes. Further studies of RF heating are required to establish the safety of EEG–fMRI for implanted electrodes.

3.7
Summary

RF heating of electrodes or brain tissue is the principal safety issue in EEG–fMRI. The degree of heating is dependent on a wide range of factors, including: the number of electrodes and their shape; lead arrangement, length and proximity to the scanner transmit coil; scanner hardware, software and scanning sequence. EEG–fMRI recordings using scalp electrodes with current limiting resistors and minimised electrode lead loops have been shown to be safe at 1.5 T. Such studies have been performed at multiple centres with scanners up to 3 T for many years with no adverse incidents reported. However, extending

these findings to body RF coils and higher field scanners requires further investigation. In particular, the effectiveness of current limiting resistors at higher RF frequencies is unclear. In view of the range and sensitivity of the factors influencing RF heating, a local risk assessment and adherence to a strict experimental protocol is essential.

References

Akca IB, Oner Ferhanoglu MS, Yeung CJ, et al. (2007) Measuring local RF heating in MRI: simulating perfusion in a perfusionless phantom. J Magn Reson Imaging 26:1228–1235

Allen PJ, Josephs O, Turner R (2000) A method for removing imaging artefact from continuous EEG recorded during functional MRI. Neuroimage 12:230–239

Allen PJ, Polizzi G, Krakow K, et al. (1998) Identification of EEG events in the MR scanner: the problem of pulse artefact and a method for its subtraction. Neuroimage 8:229–239

Anami K, Mori T, Tanaka F, et al. (2003) Stepping stone sampling for retrieving artefact-free electroencephalogram during functional magnetic resonance imaging. Neuroimage 19:281–295

Angelone LM, Potthast A, Segonne F, et al. (2004) Metallic electrodes and leads in simultaneous EEG-MRI: specific absorption rate (SAR) simulation studies. Bioelectromagnetics 25:285–295

Angelone LM, Vasios CE, Wiggins G, et al. (2006) On the effect of resistive EEG electrodes and leads during 7T MRI: simulation and temperature measurement studies. Neuroimage 24:801–812

Baker KB, Tkach JA, Nyenhuis JA, et al. (2004) Evaluation of specific absorption rate as a dosimeter of MRI-related implant heating. J Magn Reson Imaging 20:315–320

Baumann SB, Noll DC (1999) A modified electrode cap for EEG recordings in MRI scanners. Clin Neurophysiol 110:2189–2193

Benar CG, Aghakhani Y, Wang, et al. (2003) Quality of EEG in simultaneous EEG–fMRI for epilepsy. Clin Neurophysiol 114:569–580

Bonmassar G, Anami K, Ives J, et al. (1999) Visual evoked potential (VEP) measured by simultaneous 64-channel EEG and 3T fMRI. Neuroreport 10:1893–1897

Bonmassar G, Purdon PL, Jaaslelainen IP, et al. (2002) Motion and ballistocardiogram artefact removal for interleaved recording of EEG and EPs during MRI. Neuroimage 16:1127–1141

Boucousis S, Edwards J, Goodyear BG, et al. (2005) Safety and feasibility of intracranial EEG–fMRI at 3 Tesla. Epilepsia 46 S8:37 (abstract 1.071)

Brooks ML, O'Connor MJ, Sperling MR, et al. (1992) Magnetic resonance imaging in localization of EEG depth electrodes for seizure monitoring. Epilepsia 33:888–891

Carmichael DW, Pinto S, Limousin-Dowsey P, et al. (2007a) Functional MRI with active, fully implanted, deep brain stimulation systems: safety and experimental confounds. Neuroimage 37:508–517

Carmichael DW, Thorton JS, Allen PJ, et al. (2007b) Safety of localizing intracranial EEG electrodes using MRI. Proc Intl Soc Magn Reson Med 15:1073

Cohen MS, Goldman RI, Jerome E Jr (2001) Simultaneous EEG and fMRI made easy. Proc Annual Meeting of the Organization for Human Brain Mapping, Brighton, UK, 10–14 June 2001, p. 6

Collins CM, Liu W, Wang J, et al. (2004) Temperature and SAR calculations for a human head within volume and surface coils at 64 and 300 MHz. J Magn Reson Imaging 19:650–656

Davies LM, Spencer DD, Spencer SS, et al. (1999) MR imaging of implanted depth and subdural electrodes: is it safe? Epilepsy Res 35:95–98

Debener S, Mullinger KJ, Niazy RK, et al. (2007) Properties of the ballistocardiogram artefact as revealed by EEG recordings at 1.5, 3 and 7 T static magnetic field strength. Int J Pyschophysiol 67:188–199; doi:10.1016/j.ijpsycho.2007.05.015

Dempsey MF, Condon B, Hadley DM (2001) Investigation of the factors responsible for burns during MRI. J Magn Reson Imaging 13(4):627–631

Deuschl G, Eisen A (1999) Recommendations for the practice of clinical neurophysiology: guidelines of the International Federation of Clinical Neurophysiology, 2nd edn. Elsevier, Amsterdam

Garreffa G, Bianciardi M, Hagberg GE, et al. (2004) Simultaneous EEG–fMRI acquisition: how far is it from being a standardized technique? Magn Reson Imaging 22:1445–1455

Georgi JC, Lawrence AD, Mehta MA, et al. (2004) Active deep brain stimulation during MRI: a feasibility study. Magn Reson Med 51:380–388

Goldman RI, Stern JM, Engel J Jr, et al. (2000) Acquiring simultaneous EEG and functional MRI. Clin Neurophysiol 111:1974–1980

Gray RW, Bibens WT, Shellock FG (2005) Simple design changes to wires to substantially reduce MRI-induced heating at 1.5T: implications for implanted leads. Magn Reson Imaging 23:887–891

Gualniera G, Garreffa G, Morasso P, et al. (2004) A method for real-time artefact filtering during simultaneous EEG–fMRI acquisition: preliminary results. Neurocomputing 58–60:1171–1179

Hill RA, Chiappa KH, Huang-Hellinger F, et al. (1995) EEG during MR imaging: differentiation of movement artefact from paroxysmal cortical activity. Neurology 45:1942–1943

Hoffmann A, Jager L, Werhahn KJ, et al. (2000) Electroencephalography during functional echoplanar imaging: detection of epileptic spikes using post-processing methods. Magn Reson Med 44:791–798

Hofman MBM, De Cock CC, van der Linden JC, et al. (1996) Transesophageal cardiac pacing during magnetic resonance imaging: feasibility and safety considerations. Magn Reson Med 35:413–422

Huang-Hellinger FR, Breiter HC, McCormak G, et al. (1995) Simultaneous functional magnetic resonance imaging and electrophysiological recording. Hum Brain Mapp 3:13–23

Iannetti GD, Bonaventura CD, Pantano P, et al. (2002) fMRI/EEG in paroxysmal activity elicited by elimination of central vision and fixation. Neurology 58:976–979

IEC (2002a) International standard, medical equipment, part 2–33: particular requirements for the safety of magnetic resonance equipment for medical diagnosis. International Electrotechnical Commission 60601-2-33, Geneva

IEC (2002b) International standard, medical electrical equipment, part 2–26: particular requirements for the safety of electroencephalographs. International Electrotechnical Commission 60601-2-26, Geneva

IEC (2005) International standard, medical equipment, part 1: general requirements for basic safety and essential performance. International Electrotechnical Commission 60601-1:2005, Geneva

Ives JR, Warach S, Schmitt F, et al. (1993) Monitoring the patient's EEG during echo planar MRI. Electroenceph Clin Neurophysiol 87:417–420

Janssen R, Benignus VA, Grimes LM, et al. (1986) Unrecognized errors due to analog filtering of the brain-stem auditory evoked response. Electroenceph Clin Neurophysiol 65:203–211

Kainz W (2007) MR heating tests of MR critical implants. J Magn Reson Imaging 26:450–451

Kamp A, Lopes Da Silva F (1998) Technological aspects of EEG recording. In: Niedermeyer E, Lopes Da Silva F (eds) Electroencephalography. Basic principles, clinical applications and related fields, 4th edn. Williams and Wilkins, Baltimore

Kanal E, Cida Meltzer C, Adelson PD, et al. (1999) Platinum subdural grid: MR imaging compatibility testing. Radiology 211:886–888

Kruggel F, Wiggins CJ, Herrmann CS, et al. (2000) Recording of the event related potentials during functional MRI at 3.0 Tesla field strength. Magn Reson Med 44:277–282

Laufs H, Kleinschmidt A, Beyerle A, et al. (2003) EEG-correlated fMRI of human activity. Neuroimage 19:1463–1476

Lazeyras F, Zimine I, Blanke O, et al. (2001) Functional MRI with simultaneous EEG recording: feasibility and application to motor and visual activation. J Magn Reson Imaging 13:943–948

Lemieux L, Allen PJ, Franconi F, et al. (1997) Recording of EEG during fMRI experiments: patient safety. Magn Reson Med 38:943–952

Mandelkow H, Halder P, Boesiger P, et al. (2006) Synchronisation facilitates removal of MRI artefacts from concurrent EEG recordings and increases usable bandwidth. Neuroimage 32:1120–1126

Mirsattari SM, Lee DH, Jones D, et al. (2004) MRI compatible EEG electrode system for routine use in the epilepsy monitoring unit and intensive care unit. Clin Neurophysiol 115:2175–2180

Negishi M, Abildgaard M, Nixon T, et al. (2004) Removal of time varying gradient artefacts from EEG data acquired during continuous fMRI. Clin Neurophysiol 115:2181–2192

Nuwer MR, Comi G, Emerson R et al (1999) IFCN standards for digital recording of clinical EEG. In: Deuschl G, Eisen A (eds) Recommendations for the practice of clinical neurophysiology: guidelines of the International Federation of Clinical Neurophysiology, 2nd edn. Elsevier, Amsterdam

Park SM, Nyenhuis JA, Smith CD, et al. (2003) Gelled versus nongelled phantom material for measurement of MRI-induced temperature increases with bioimplants. IEEE Trans Magn 39:3367–3371

Pictet J, Meuli R, Wicky S, et al. (2000) Radiofrequency heating effects around resonant lengths of wire in MRI. Phys Med Biol 47:2973–2985

Rezai AR, Finelli D, Nyenhuis JA, et al. (2002) Neurostimulation systems for deep brain stimulation: in vitro evaluation of magnetic resonance imaging-related heating at 1.5T. J Magn Reson Imaging 15:241–250

Roth BJ, Pascual-Leone A, Cohen LG, et al. (1992) The heating of metal electrodes during rapid-rate magnetic stimulation: a possible safety hazard. Electroenceph Clin Neurophysiol 85:116–123

Seeck M, Lazeyras F, Michel CM, et al. (1998) Non-invasive epileptic focus localization using EEG-triggered functional MRI and electromagnetic tomography. Electroenceph Clin Neurophysiol 106:508–512

Shellock FG (2007) Comments on MR heating tests for critical implants. J Magn Reson Imaging 26:1182–1185

Srivastava G, Crottaz-Herbette S, Lau KM, et al. (2005) ICA-based procedures for removing ballistocardiogram artefacts from EEG data acquired in the MRI scanner. Neuroimage 24:50–60

Stevens TK, Ives JR, Martyn Klassen L, et al. (2007) MR compatibility of EEG electrodes at 4 Tesla. J Magn Reson Imaging 25:872–877

Van Audekerke J, Peeters R, Verhoye M, et al. (2000) Special designed RF-antenna with integrated non-invasive carbon electrodes for simultaneous magnetic resonance imaging and electroencephalography acquisition at 7T. Magn Reson Imaging 18:887–891

Van Genderingen HR, Sprenger M, de Ridder JW, et al. (1989) Carbon-fiber electrodes and leads for electrocardiography during MR imaging. Radiology 171:872

Vasios CE, Angelone LM, Purdon PL, et al. (2006) EEG/(f)MRI measurements at 7 Tesla using a new EEG cap ("Inkcap"). Neuroimage 33:1082–1092

Warach S, Ives JR, Schlaug G, et al. (1996) EEG-triggered echo-planar functional MRI in epilepsy. Neurology 47:89–93

Woods TO (2007) Standards for medical devices in MRI: present and future. J Magn Reson Imaging 26:1186–1189

Yeung CJ, Susil RC, Atalar E (2002) RF safety index of wires in interventional MRI: using a safety index. Magn Reson Med 47:187–193